Competition between the Bénard-Marangoni and the Rosensweig Instability in Magnetic Fluids

Jochen Weilepp, Helmut Brand

Competition between the Bénard-Marangoni and the Rosensweig Instability in Magnetic Fluids

Jochen Weilepp and Helmut R. Brand(*)

Theoretische Physik III, Universität Bayreuth, D-95440 Bayreuth, Germany

(Received 17 July 1995, revised 20 October 1995, accepted 15 December 1995)

PACS.75.50.Mm – Magnetic liquids
PACS.47.20.Dr – Surface-tension-driven instability
PACS.05.70.Ln – Nonequilibrium thermodynamics, irreversible processes

Abstract. — The linear stability analysis of a layer of a magnetic fluid with a deformable free surface, which is heated from below and exposed to a uniform, vertically applied magnetic field is presented. In this configuration the temperature dependence of the surface tension, the buoyancy and the focusing of the magnetic field due to surface fluctuations act as destabilising effects. We show that this system has for thin layers a stationary codimension–2–point, which can be reached for experimentally relevant values of the material parameters. We also analyse the transition from thin to thicker layers for which there is no codimension–2–point and we show how the codimension–2–point disappears. Finally we demonstrate that there is no oscillatory instability in the regions of parameter space considered here.

1. Introduction

A planar horizontal layer of a fluid becomes unstable when heated from below provided a sufficiently high temperature gradient is applied. The first analysis carried out by Rayleigh [1] to determine the onset of thermal convection considered the buoyancy force as the destabilising mechanism giving rise to thermal convection. The applied temperature gradient induces an adverse density gradient, which is caused by thermal expansion in the heat conduction state. At a certain critical temperature gradient the destabilising forces are strong enough to overcome the stabilising viscous forces and thermal diffusion, so that small fluctuations grow and stationary convective motion sets in (*Rayleigh–Bénard instability*). Buoyancy forces turned out to be the dominant effect to drive convection for rigid boundaries. The same calculations carried out for a thin ($d \approx 1$ mm) layer with a free surface showed that buoyancy effects are not sufficient to account for the experimental results of Bénard [2]. Pearson [3] proposed another effect to drive convection, namely surface tension, which is a monotonically decreasing function of temperature for most fluids. Fluid particles reaching the surface with higher temperature because of small fluctuations, induce a gradient in surface temperature and thus an adverse destabilising gradient in surface tension arises. The applied temperature gradient becomes critical when it is strong enough to overcome viscous forces and thermal diffusion: stationary convection sets in (*Bénard–Marangoni instability*). This phenomenon turns out to provide the

(*) Author for correspondence (e-mail: btp511@btp3x6.phy.uni-bayreuth.de)

relevant mechanism for the onset of the convective motion observed by Bénard. Pearson also pointed out, that the influence of buoyancy effects becomes dominant for thicker layers (about $d \approx 1$ cm). Nield [4] first considered both effects and described how they interact at the threshold of the instability. The influence of buoyancy effects becomes dominant for thicker layers (about $d > 5$ mm), as already stated by Pearson [3], but not investigated in detail. While the early calculations were done for nondeformable surfaces and focusing exclusively on stationary onset, later these assumptions were dropped (compare, for example, Refs. [5-11]).

While the Rayleigh-Bénard and the Bénard-Marangoni instability discussed up to now arise in many fluids, we want to focus here on magnetic liquids, suspensions of small magnetic monodomain particles (diameter $d \sim 100$ Å) in a carrier fluid [12,13]. Due to the large Brownian motion of the suspended particles these liquids do not have a spontaneous magnetisation, but show a strong response to small magnetic fields [12, 13]. A vertically applied, uniform and static magnetic field has a destabilising influence on the free surface of a magnetic fluid, since the boundary conditions for magnetic field and magnetic induction lead to a focusing of the magnetic field along the wave crests on the surface slightly disturbed by small fluctuations. Thus a destabilising gradient of the magnetic field in the fluid in the vicinity of the surface arises. As shown first by Cowley and Rosensweig [14] the surface becomes unstable, when the influence of the magnetic forces overcomes the stabilising forces associated with gravity and surface tension (*Rosensweig instability*). The surface deforms and generates a triangular array of peaks, standing statically in the fluid. In contrast to the dissipative Bénard-Marangoni instability discussed above, the Rosensweig instability is static and is the result of a balance of several contributions to the total energy, namely of the magnetic energy, the energy in the gravitational field and the surface energy. We note that a similar energy balance and thus the same type of instability arises, when an electric field is applied perpendicularly to the surface of a liquid metal (compare Ref. [15] for a comprehensive treatment of this instability). Time-dependent behavior occurs only during the short transient periods when the external magnetic field is changed. The main difference between the convective instabilities mentioned above and the Rosensweig instability is thus, that the former shows stationary flows, while the latter is static.

This key difference between the two types of instabilities raises the question how the system behaves, when applying both a temperature gradient and a magnetic field to the free surface of a magnetic liquid. In the following we address this issue and describe the results of a linearised stability analysis. The paper is organised as follows: in Section 2 we formulate the problem and in Sections 3 and 4 we analyse in detail the stationary and the oscillatory instability, respectively, followed by the conclusion in Section 5.

2. Formulation of the Problem

We consider a flat, horizontally unbounded layer of a viscous magnetic fluid with finite depth d (medium 2; see Fig. 1 for a sketch of the set-up), which is bounded below ($z = 0$) by a planar, rigid plate of constant temperature and has a deformable free surface described by the function $z = d + \zeta(x, y, t)$. The system is heated from below and a uniform magnetic field is applied vertically to the flat surface. For simplicity we assume the media outside the fluid to be vacuum. Surface tension σ and density ρ are assumed to depend linearly on temperature T:

$$\sigma(T) = \sigma(T_R) - \gamma(T - T_R) \qquad \rho(T) = \rho(T_R) - \alpha(T - T_R) \tag{1}$$

where $\gamma = -(\partial\sigma(T)/\partial T)_{T=T_R}$ represents the rate of change in surface tension due to temperature variations and $\alpha = -(\partial\rho(T)/\partial T)_{T=T_R}$ is the coefficient of volume expansion. Both

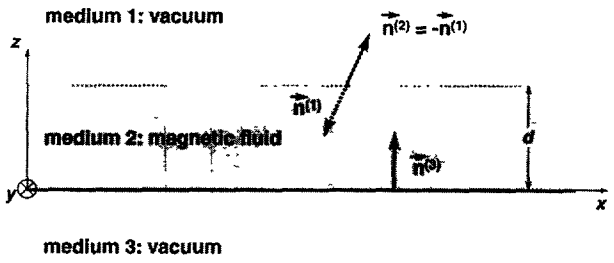

Fig. 1. — Sketch of the considered set-up.

coefficients are taken at the reference temperature T_{R}. We concentrate on homogeneous magnetic fields and on thin layers. In this case (i.e. $d \propto 1$ mm) the Marangoni effect provides the dominant mechanism to drive convection. Then a temperature gradient of about 1 Kmm^{-1} is sufficient to drive Bénard–Marangoni convection, whereas a temperature gradient of about $10-100\,\mathrm{Kmm}^{-1}$ is necessary for Rayleigh–Bénard convection. Estimates show that the contribution of the magnetothermal effect to thermoconvection (this mechanism is discussed in detail in [16,17]; there it is shown that the threshold of magnetothermal convection in homogeneous fields is $\propto (\Delta T)^2 d^2$) for the considered thicknesses of the fluid layers is much smaller than that of buoyancy and thus can be neglected.

Furthermore, we assume the magnetic fluid to be electrically insulating, so that the stationary magnetic Maxwell equations reduce to Laplace equations for the magnetic potentials $\Phi^{(i)}$ (magnetic field: $\mathbf{H}^{(i)} = \nabla\phi^{(i)}$; upper indices in round brackets denote the medium which is considered) for the three different regions. In addition we assume the magnetic fluid to be homogeneous and isotropic and to react linearly to an applied magnetic field (cf. [12] where these assumptions are discussed), i.e. $\mathbf{M} = (1+\mu_{\mathrm{r}})\,\mathbf{H}^{(2)}$, with the magnetisation in the fluid $\mathbf{M}$, and its relative permeability μ_{r} .

The bulk equations to describe our system are given by (Boussinesq–approximation):

$$\operatorname{div}\mathbf{v} = 0 \tag{2}$$

$$\partial_t\mathbf{v} + (\mathbf{v}\cdot\nabla)\,\mathbf{v} = -\frac{1}{\rho}\nabla\Pi + \nu\Delta\mathbf{v} + \frac{g\alpha}{\rho}(T-T_{\mathrm{R}})\,\mathbf{e}_z \tag{3}$$

$$\partial_t T + \mathbf{v}\cdot\nabla T = \chi\Delta T \tag{4}$$

$$\Delta\Phi^{(i)} = 0 \tag{5}$$

with the velocity $\mathbf{v} = (u,v,w)$, the density of the fluid ρ and its kinematic viscosity ν, the acceleration due to gravity g, the unit vector in vertical direction $\mathbf{e}_z$, the coefficient of thermal diffusivity χ and the expression $\Pi = p + p_{\mathrm{s}} + \rho g z$, which contains various contributions to the pressure. The *magnetostrictive pressure* $p_{\mathrm{s}} = -\mu_0 \int_0^{H^{(2)}} \rho\,(\partial M/\partial\rho)_{H,T}\,\mathrm{d}H$, ($H$ and M denote the moduli of magnetic field and magnetisation in the fluid) is due to the fact that we consider magnetic fluids (cf. [12]).

Most of the effects discussed here are induced by the boundaries. First we have to consider the boundary conditions for the magnetic field $\mathbf{H}$ and the magnetic induction $\mathbf{B}$:

$$\mathbf{n}\times[\mathbf{H}] = 0 \quad \text{and} \quad \mathbf{n}\cdot[\mathbf{B}] = 0\,, \tag{6}$$

where the brackets denote the difference of the function inside at both sides of the boundary. We assume a rigid plate at constant temperature T_{B} as lower boundary ($z = 0$). The corresponding

boundary conditions read:

$$\mathbf{v} = 0\,; \qquad \partial_z w = 0\,; \qquad T = T_B\,. \tag{7}$$

The free surface at $z = d + \zeta(x,y,t)$ is assumed to be stress–free, so that the stress difference in the media 1 and 2 is balanced by the capillary stress $\mathbf{p}_c$.
The stress tensor $T_{ij}^{(2)}$ of an incompressible and viscous magnetic fluid [12] reads:

$$T_{ij}^{(2)} = -\left\{ p + \int_0^H \mu_0 \left(\frac{\partial(MV)}{\partial V} \right)_{H\,T} \mathrm{d}H + \frac{1}{2}\mu_0 H^2 \right\} \delta_{ij} + B_i H_j + \rho\nu\,(\partial_i v_j + \partial_j v_i)\,. \tag{8}$$

Assuming vacuum as medium 1, the equilibrium condition $\left(n_i \left(T_{ij}^{(1)} - T_{ij}^{(2)}\right) + (\mathbf{p}_c)_j = 0\right)$ reduces – taking into account conditions (6) (cf. [12]) – to the following nonlinear form:

$$\mathbf{n} \cdot \left\{ (p + p_s + p_m + p_n)\, I - \rho\nu \left(\boldsymbol{\nabla}\mathbf{v} + (\boldsymbol{\nabla}\mathbf{v})^T \right) \right\} - \mathbf{p}_c = 0 \tag{9}$$

with the unit vector normal to the surface:

$$\mathbf{n} = \frac{\boldsymbol{\nabla}\,(z - \zeta(x,y,t))}{\sqrt{1 + (\boldsymbol{\nabla}\zeta)^2}}$$

and the following contributions to the total pressure: $p_m = \mu_0 \int_0^{H^{(2)}} M\,\mathrm{d}H$, $p_n = \frac{1}{2}\mu_0 M_n^2$ and $\mathbf{p}_c = -\sigma\mathbf{n}\,(\boldsymbol{\nabla}\cdot\mathbf{n}) - \gamma\boldsymbol{\nabla}_t T$, where $\boldsymbol{\nabla}_t = \boldsymbol{\nabla} - \mathbf{n}\,(\mathbf{n}\cdot\boldsymbol{\nabla})$ denotes the gradient tangential to the surface. I is the unity tensor.
At a deformable free surface the z-component of the velocity is related to the surface deflection $\zeta(x,y,t)$ by the kinematic boundary condition:

$$w\big|_{z=d+\zeta} = \partial_t \zeta + \mathbf{v}\cdot\boldsymbol{\nabla}\zeta\,. \tag{10}$$

We assume the heat flux Q through the surface to be proportional to the local temperature gradient:

$$Q(T) = -\kappa\,\mathbf{n}\cdot\boldsymbol{\nabla}T \tag{11}$$

with the coefficient of heat conduction κ. Following the usual steps of a linear stability analysis (see e.g. [18]) and choosing d, d^2/ν, $\nu^2\rho/d^2$, $(T_B - T_S)\nu/\chi$, $q(T_B - T_S)\nu/\chi$, M_0 (magnetisation of the fluid in the groundstate) and $M_0 d$ as the units of length, time, pressure, temperature, heat flux, magnetisation (and magnetic field) and magnetic potential respectively, we obtain the corresponding linearised, dimensionless perturbation equations and boundary conditions. Here $q = (\partial Q/\partial T)_{T=T_R}$ represents the rate of change in heat flux due to temperature variations at a reference temperature, T_B and T_S are the temperatures at the bottom plate and at the deformable free surface, respectively.
The dimensionless magnetic boundary value problem:

$$\Delta\Phi_1^{(i)} = 0 \quad \text{for the media } i = 1,2,3 \tag{12}$$

with:

$$\partial_{x(y)} \left(\Phi_1^{(2)} - \Phi_1^{(3)} \right) = \partial_z \left(\mu_r \Phi_1^{(2)} - \Phi_1^{(3)} \right) = 0 \quad \text{at } z = 0 \tag{13}$$

and

$$\partial_{x(y)} \left(\Phi_1^{(1)} - \Phi_1^{(2)} \right) + \partial_{x(y)}\zeta_1 = \partial_z \left(\Phi_1^{(1)} - \mu_r \Phi_1^{(2)} \right) = 0 \quad \text{at } z = 1\,, \tag{14}$$

decouples from the flow problem and can be solved separately.
The perturbative potentials $\Phi_1^{(i)}$ (the subscript '1' denotes perturbative quantities) and the surface deflection ζ_1 (and later on also the velocity w_1, pressure Π_1 and temperature θ_1) are analysed in normal modes of the following form:

$$O(x,y,z,t) = \hat{O}(z) \exp\{i(k_x x + k_y y + \omega t) + at\} \; + \; \text{c.c.}\,, \tag{15}$$

where O denotes one of the above quantities, hats denote amplitudes which are independent of the lateral coordinates x and y, ω is the dispersion, a the growth rate and c.c. denotes the complex conjugate. The components of the wave vector are related to the wave number by $k = \sqrt{k_x^2 + k_y^2}$. With this ansatz we obtain for the potential $\Phi_1^{(2)}$ in the magnetic fluid:

$$\Phi_1^{(2)} = \phi^{(2)}\, \zeta_1\, \mathrm{e}^{kz} \; + \; \tilde{\phi}^{(2)}\, \zeta_1\, \mathrm{e}^{-kz} \tag{16}$$

with

$$\begin{aligned} \phi^{(2)} &= \frac{(1+\mu_\mathrm{r})\,\mathrm{e}^{k}}{(1+\mu_\mathrm{r})^2\,\mathrm{e}^{k} - (1-\mu_\mathrm{r})^2\,\mathrm{e}^{-k}} \\ \tilde{\phi}^{(2)} &= -\frac{(1-\mu_\mathrm{r})\,\mathrm{e}^{-k}}{(1+\mu_\mathrm{r})^2\,\mathrm{e}^{k} - (1-\mu_\mathrm{r})^2\,\mathrm{e}^{-k}} \end{aligned} \tag{17}$$

Following the usual steps (e.g. [18]) using the normal modes (Eq. (15)) and taking into account equation (16), the remaining problem to determine the onset of instability ($a = 0$) reads:

α) Bulk equations:

$$\left(D^2 - k^2\right)\left(D^2 - k^2 - i\omega\right)\hat{w}_1(z) \;=\; \mathcal{R}k^2\,\hat{\theta}_1(z) \tag{18}$$

$$\left(i\omega\mathcal{P} - D^2 + k^2\right)\hat{\theta}_1(z) \;=\; \hat{w}_1(z) \tag{19}$$

β) Boundary conditions:

$z = 0$:

$$\hat{w}_1 = D\hat{w}_1 = \hat{\theta}_1 = 0 \tag{20}$$

$z = 1$:
tangential stress balance:

$$\left(D^2 + k^2\right)\hat{w}_1 = -\,\mathcal{M}k^2\left(\hat{\theta}_1 \; - \; \mathcal{P}^{-1}\hat{\zeta}_1\right) \tag{21}$$

normal stress balance:

$$\mathcal{C}\mathcal{P}\left(i\omega - D^2 + 3k^2\right)D\hat{w}_1 + \left[\left(\mathcal{B} + k^2\right)k^2 \; - \; \mathcal{N}\Lambda(k)k^3\right]\hat{\zeta}_1 \;=\; 0 \tag{22}$$

kinematic boundary condition:

$$\hat{w}_1 = i\omega\hat{\zeta}_1 \tag{23}$$

thermal boundary condition:

$$(D + \mathcal{L})\,\hat{\theta}_1 = \mathcal{L}\mathcal{P}^{-1}\hat{\zeta}_1 \tag{24}$$

where $D = \mathrm{d}/\mathrm{d}z$ and where the following dimensionless numbers have been introduced: Rayleigh number $\mathcal{R} = \tau_\mathrm{t}\tau_\mathrm{v}/\tau_\mathrm{b}^2 = g\alpha\Delta T d^3/(\chi\nu)$, Prandtl number $\mathcal{P} = \tau_\mathrm{t}/\tau_\chi = \nu/\chi$, Crispation number $\mathcal{C} = \tau_\mathrm{s}^2/(\tau_\mathrm{t}\tau_\chi) = \rho\nu\chi/(d\sigma)$, Bond number $\mathcal{B} = \tau_\mathrm{s}^2/\tau_\mathrm{g}^2 = g\rho d^2/\sigma$, Marangoni number $\mathcal{M} = \tau_\mathrm{t}\tau_\chi/\tau_\mathcal{M}^2 = \gamma\Delta T d/(\rho\chi\nu)$, and magnetisation number $\mathcal{N} = \tau_\mathrm{s}^2/\tau_\mathrm{m}^2 = \mu_0\mu_\mathrm{t}M^2 d/\sigma$ (with the following relaxation timescales: viscous timescale: $\tau_\chi = d^2/\nu$, thermal timescale: $\tau_\mathrm{t} = d^2/\chi$, buoyancy timescale: $\tau_\mathrm{b}^2 = d/(\alpha\Delta T g)$, surface tension timescale $\tau_\mathrm{s}^2 = \rho d^3/\sigma$, gravitation timescale $\tau_\mathrm{g}^2 = d/g$, timescale due to the Marangoni-effect $\tau_\mathcal{M}^2 = \rho d^3/(\gamma\Delta T)$ and magnetisation timescale $\tau_\mathrm{m}^2 = \rho d^2/(\mu_0\mu_\mathrm{t}M^2)$). The Biot number $\mathcal{L}$ is defined as the additional heat flux through the surface due to temperature fluctuations divided by the heat flux through the surface in the basic state: $\mathcal{L} = qd/\kappa$. The function $\Lambda(k)$ is given by

$$\Lambda(k) = \frac{\mathrm{e}^k(1+\mu_\mathrm{t}) + \mathrm{e}^{-k}(1-\mu_\mathrm{t})}{\mathrm{e}^k(1+\mu_\mathrm{t})^2 - \mathrm{e}^{-k}(1-\mu_\mathrm{t})^2}.$$

3. Stationary Instability

In this section we analyse in detail the stationary case ($\omega = 0$). The associated linear boundary value problem given by equations (18)-(24) is solved by a linear combination of complex hyperbolic functions (for details see appendix A). Implementing the boundary conditions we obtain a homogeneous (6×6) set of linear equations, which has a nontrivial solution if and only if the coefficient determinant vanishes. This condition yields the neutral curves. In our system the applied magnetic field and the temperature gradient are the two parameters that can be controlled well experimentally. Since the latter appears in both the Marangoni number $\mathcal{M}$ and the Rayleigh number $\mathcal{R}$, it is more convenient to determine the neutral curves for the magnetisation number $\mathcal{N}(k)$ and treat the temperature gradient as a parameter. We obtain (cf. appendix A):

$$\mathcal{N}(k) = \frac{1}{\Lambda(k)k^3}\left[\left(\mathcal{B}+k^2\right)k^2 + g(\mathcal{R},\mathcal{M},\mathcal{C},\mathcal{L},k)\right] \tag{25}$$

where $g(\mathcal{R},\mathcal{M},\mathcal{C},\mathcal{L},k)$ is given in the appendix.

3.1. Limiting Cases

3.1.1. Rayleigh-Bénard and Bénard-Marangoni Instability. – As we consider neutral curves of equation (25) pure thermal instabilities set in, when there are zeros of the function $\mathcal{N}(k)$ (note that $\mathcal{N}$ cannot become negative by construction). To evaluate the neutral curves we have used two methods. In addition to the method outlined above and discussed in detail in appendix A we have also used that of Nield [4] which is also applicable for $\mathcal{R} = 0$.
From our calculations of the neutral curves $\mathcal{M}(k)$ we recover as special cases the results obtained by Pearson [3], Nield [4], Lebon and Cloot [19], Takashima [7] and Pérez García and Carneiro [9] for Bénard-Marangoni convection.

3.1.2. Rosensweig Instability for Layers of Finite Thickness. – The other special case contained in equation (25) are isothermal conditions ($\hat{\theta}_1 = 0$) giving rise to the Rosensweig instability. The linear boundary value problem for this case reduces to:

$$\left(D^2-k^2\right)\left(D^2-k^2-\imath\omega\right)\hat{w}_1(z) = 0\,. \tag{26}$$

$$\hat{w}_1 = D\hat{w}_1 = 0 \qquad \text{at } z = 0 \tag{27}$$

$$\mathcal{C}\mathcal{P}\left(\imath\omega - D^2 + 3k^2\right)D\hat{w}_1 + \left(\mathcal{B}+k^2\right)k^2\hat{\zeta}_1 - \mathcal{N}\Lambda(k)k^3\hat{\zeta}_1 = 0$$

$$\left(D^2+k^2\right)\hat{w}_1 = 0 \qquad \hat{w}_1 = \imath\omega\hat{\zeta}_1 \quad \text{at } z = 1 \tag{28}$$

The solution of (26) can be written in the following form:

$$\hat{w}_1 = A_1 \sinh(\lambda_1 z) + A_2 \sinh(\lambda_2 z) + B_1 \cosh(\lambda_1 z) + B_2 \cosh(\lambda_2 z)\,. \tag{29}$$

with $\lambda_1 = k$ $\lambda_2 = \sqrt{k^2 + i\omega}$

and $A_1 = -K_2 B_2$ $A_2 = K_1 B_2$ $B_1 = -\left(1 + \dfrac{i\omega}{2k^2}\right) B_2$

where
$$K_1 = \frac{\sinh(-\lambda_1)}{\cosh(-\lambda_2)} \cdot \frac{\lambda_1 \tanh(-\lambda_1) - \lambda_1 \coth(-\lambda_1)}{\lambda_2 \tanh(-\lambda_1) - \lambda_1 \tanh(-\lambda_2)} \left(1 + \frac{i\omega}{2k^2}\right) - \tanh(-\lambda_2) \frac{\lambda_2 \tanh(-\lambda_1) - \lambda_1 \coth(-\lambda_2)}{\lambda_2 \tanh(-\lambda_1) - \lambda_1 \tanh(-\lambda_2)}$$

$$K_2 = \frac{\sinh(-\lambda_2)}{\sinh(-\lambda_1)} K_1 - \coth(-\lambda_1) \left(1 + \frac{i\omega}{2k^2}\right) + \frac{\cosh(-\lambda_2)}{\sinh(-\lambda_1)}\,. \tag{30}$$

This yields the following dispersion relation:

$$\mathcal{CP}\left[2\left(K_1\sqrt{k^2 + i\omega} - K_2 k\right)k^2 - iK_2\omega k\right] - \frac{1}{2}\left(\mathcal{B} + k^2 - \mathcal{N}\Lambda(k)k\right) = 0\,. \tag{31}$$

For an infinite thickness of the layer this reads:

$$\left(1 + \frac{i\omega}{2k^2}\right)^2 + \frac{1}{4\mathcal{CP}k^3}\left(\mathcal{B} + k^2 - \frac{\mathcal{N}}{1+\mu_1}\right) = \sqrt{1 + \frac{i\omega}{k^2}} \tag{32}$$

which is discussed in [20].
In the limiting case $\omega = 0$ we obtain the condition for marginal stability:

$$\mathcal{B} + k^2 - \mathcal{N}\Lambda(k)k = 0\,. \tag{33}$$

which can also be easily derived numerically from equation (25) (g vanishes rapidly for small Rayleigh numbers $\mathcal{R}$ and Marangoni numbers $\mathcal{M}$).
For the case of an inviscid fluid the dispersion relation reduces to:

$$\omega'^2 \rho \coth(k'd) = \rho g k' + \sigma k'^3 - \mu_0 \mu_1 M_0^2 \Lambda(k'd) k'^2 \tag{34}$$

In equation (34) we returned to quantities with dimensions (the corresponding wavenumbers and dispersions are marked with a prime; in the function $\Lambda(k)$ the dimensionless k's have to be replaced by $k'd$), since the viscous timescale is no longer the appropriate one. For an infinite thickness $d \to \infty$ of the layer, relation (34) reduces to that of Rosensweig (cf. [12]). In Figure 2 the dispersion relations for a layer of the magnetic fluid EMG 901 (cf. Tab. I, where all the relevant physical data of EMG 901 are listed [21]) with the thickness $d = 1$ mm are plotted. Figure 3 shows the critical dispersion relations for different thicknesses of the fluid layer. These figures recover those of Rosensweig [12] or Néron de Surgy, Chabrerie, Denoux and Wesfreid [15], where the influence of thickness and viscosity on the electric equivalent of the Rosensweig instability in liquid metals is discussed in detail. The curves for the different thicknesses in Figure 3 all show a similar behaviour and all have a region of anomalous dispersion. There is only one qualitative difference between the curves for finite and for infinite thicknesses (which is represented here by $d = 500$ mm): the slope at $k' \to 0$. While the slope is zero for finite thickness, it is nonzero for the infinite case. This thickness effect has been observed recently

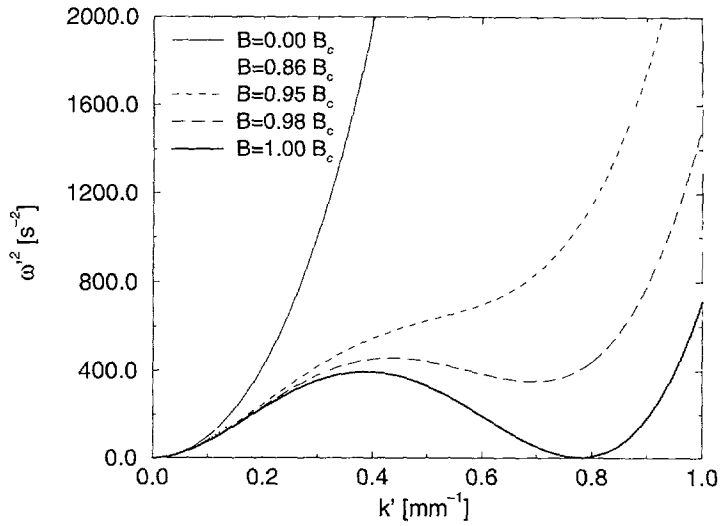

Fig. 2 — Dispersion relations for various magnetic fields (inviscid case; $d = 1$ mm).

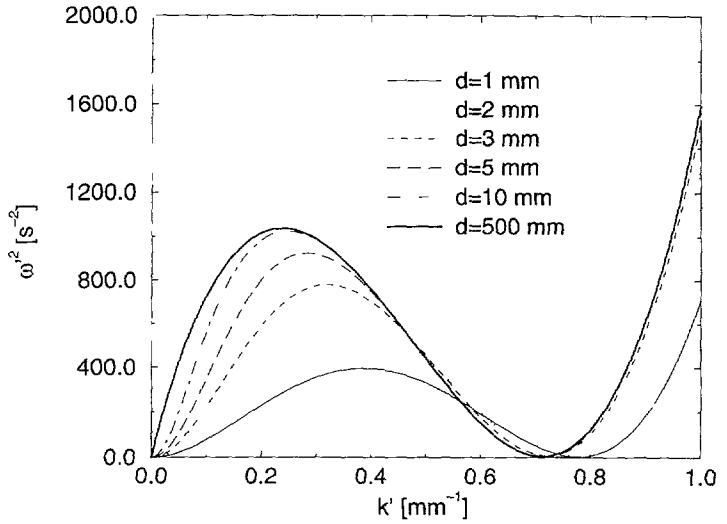

Fig. 3. — Critical dispersion relations for various thicknesses of the layer d (inviscid case)

in [22], where an experiment to measure the dispersion relation of magnetic fluids is described. The authors of reference [22] chose a V-shaped cylindrical channel with $d = 6$ mm. Interestingly they were able to show the anomalous behaviour of the dispersion relation slightly below the onset of instability.

As it is discussed in detail in [12] the onset of the Rosensweig instability is characterised by $\omega'^2 = 0$ and $d\omega'^2/dk' = 0$, which shows that the principle of the exchange of stability strictly holds for the inviscid case. It can be seen in Figure 3 and also from the plots in [15] that the critical wavenumber of the Rosensweig instability depends only slightly on the thickness

Table I. — *Physical data of the magnetic fluid EMG 901. All parameters except ˣ are taken from reference [21]. ˣ is the specific heat from EMG 905 [16] which has the same carrier liquid as EMG 901. The temperature of measurement is given when known.*

density ρ	$1.53 \times 10^3 \frac{\mathrm{kg}}{\mathrm{m}^3}$
kinematic viscosity ν (at 300 K)	$6.5 \times 10^{-6} \frac{\mathrm{m}^2}{\mathrm{s}}$
thermal conductivity κ	$1.85 \times 10^{-1} \frac{\mathrm{W}}{\mathrm{m} \cdot \mathrm{K}}$
specific heat c_p ˣ	$1.47 \times 10^3 \frac{\mathrm{J}}{\mathrm{kg} \cdot \mathrm{K}}$
thermal diffusivity χ	$8.2 \times 10^{-8} \frac{\mathrm{m}^2}{\mathrm{s}}$
coefficient of volume expansion α	$6 \times 10^{-4}\,\mathrm{K}^{-1}$
magnetic permeability μ_r	2.3
surface tension σ	$29.5 \times 10^{-3}\,\mathrm{Nm}^{-1}$
negative rate of change of surface tension with temperature $\gamma = -\frac{\partial \sigma}{\partial T}$	$7 \times 10^{-5} \frac{\mathrm{N}}{\mathrm{m} \cdot \mathrm{K}}$
capillary wavenumber $k_\mathrm{cap} := \sqrt{\frac{\rho g}{\sigma}}$	$0.713\,\mathrm{mm}^{-1}$
Rayleigh number $\mathcal{R}$	$11.0\,\mathrm{mm}^{-3}\mathrm{K}^{-1} \cdot d^3\,\Delta T$
Marangoni number $\mathcal{M}$	$85.8\,\mathrm{mm}^{-1}\mathrm{K}^{-1} \cdot d\,\Delta T$
Prandtl number $\mathcal{P}$	79.3
Biot number $\mathcal{L}$	$0.0003\,\mathrm{mm}^{-1} \cdot d$
magnetisation number $\mathcal{N}$	$9.8 \times 10^{-8} \frac{\mathrm{m}^2}{\mathrm{mm} \cdot A^2} \cdot d\,M^2$
Crispation number $\mathcal{C}$	$2.74 \times 10^{-5}\,\mathrm{mm} \cdot d^{-1}$
Bond number $\mathcal{B}$	$0.508\,\mathrm{mm}^{-2} \cdot d^2$

of the layer. Figure 4 shows the critical wavenumber scaled by the capillary wavenumber $k_\mathrm{cap} := \sqrt{\frac{\rho g}{\sigma}}$, which is obtained for $d \to \infty$, as a function of the layer thickness for the magnetic fluid EMG 901. We can see that there is only a slight correction to the capillary wavenumber in the vicinity of $d = 0.5$ mm. The maximum deviation is about 12 %. The critical induction field is nearly constant for large layer thickness and grows monotonically for smaller thicknesses

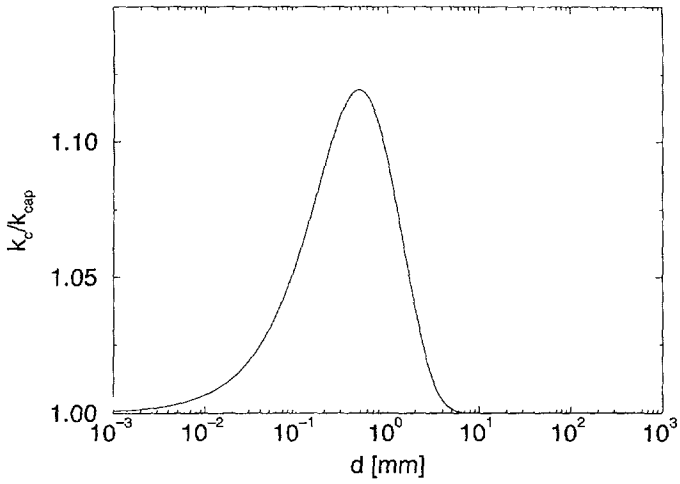

Fig. 4. – Dimensionsless critical wavenumber k_c/k_{cap} as a function of the thickness of the layer d.

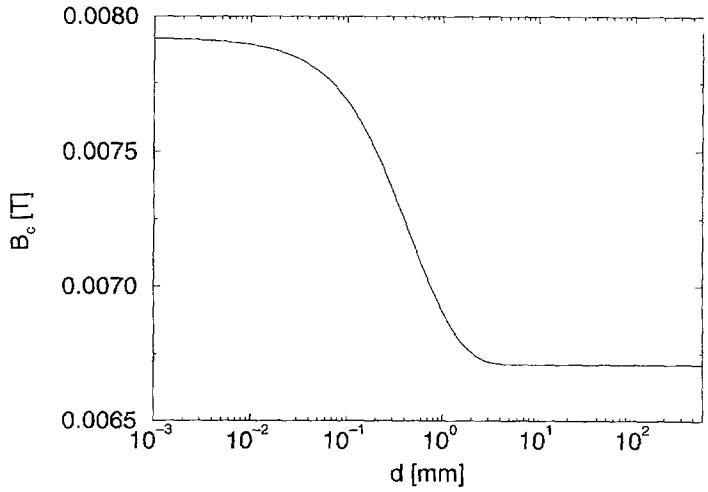

Fig. 5 – Critical magnetic induction as a function of the thickness of the layer d.

(cf. Fig. 5). This increase reflects the fact, that 'there is not enough space for the magnetic field gradient to develop completely and so the applied field has to be increased to reach the onset of the instability. But we would like to stress that this region of thin layers ($\lesssim 100\ \mu$m) is not easy to reach experimentally, because eventually surface roughness of the bottom plate becomes important. To sum up, the Rosensweig instability can be considered to be a characteristic instability shown by magnetic fluids.

Figures 4 and 5 also apply to the viscous case, since the condition for instability (33) is still the same as that for inviscid fluids. This indicates that the velocity has to vanish identically at the threshold. We demonstrate this by calculating the eigenfunctions for the stationary case.

To achieve this we have to modify solution (29) in the following way:

$$\hat{w}_1 = C_1 \sinh(kz) + C_2 \cosh(kz) + C_3 z \sinh(kz) + C_4 z \cosh(kz) , \tag{35}$$

where the coefficients C_i can be determined by the boundary conditions (27) and (28). We obtain $C_i \equiv 0$, which shows (taking into account the continuity equation) that the Rosensweig instability sets in with vanishing velocity and stresses the reversibility of the interacting mechanisms.

3.2. RESULTS FOR THE GENERAL CASE. — To be definite and since we are interested in effects, that are accessible experimentally, we present our analysis for the physical data of the magnetic fluid EMG 901 which is commercially available (cf. Tab. I, where the physical data and the corresponding dimensionless parameters of EMG 901 are listed). The exact value for the Biot number is hard to determine and differs for each experimental set-up. Nevertheless a lower bound for the Biot number $\mathcal{L}$ can be estimated roughly by means of the *Stefan–Boltzmann law* when considering a massless, inert gas with a temperature of 300 K in contact with a fluid surface at a temperature of 299 K. As a result we find the value $\mathcal{L} = 0.0003\,\mathrm{mm}^{-1}\ d$ (cf. [23]). In [9] it is mentioned, that for experimentally relevant conditions (where convection and thermal diffusion are the dominant mechanisms to transport energy) average Biot numbers are $\mathcal{L} < 0.1$.

First we restrict our analysis on the regime dominated by the Marangoni–effect and fix the layer thickness to $d = 1$ mm. By solving $\mathcal{N}(k) = 0$ we determine the critical values for the thermoconvective instability to be $\mathcal{M}_{c(\mathrm{RBM})} = 78.486$, which corresponds to $\mathcal{R} = 10.062$ and $k_{c(\mathrm{RBM})} = 1.992$ (for comparison, the critical parameters for $\mathcal{R} = 0$ are: $\mathcal{M}_{c(\mathrm{BM})} = 79.591$ and $k_{c(\mathrm{BM})} = 1.992$ and for $\mathcal{M} = 0$: $\mathcal{R}_{c(\mathrm{RB})} = 669.04$ and $k_{c(\mathrm{RB})} = 2.086$), where the index 'c' denotes critical values, 'RBM' stands for Bénard–Marangoni instability, where the Rayleigh–Bénard effect is also considered. The latter is excluded when the parameters are marked with 'BM'. Later on parameters, that correspond to the pure Rosensweig instability will carry the index 'Ro'.

In Figure 6 the neutral curves $\mathcal{N}(k)$ are plotted for different values of $\mathcal{M}$. The wavenumber is scaled with the critical wavenumber $k_{c(\mathrm{RBM})}$ for the onset of the thermal instability.

For $\mathcal{M} < 0.95\mathcal{M}_{c(\mathrm{RBM})}$ the curve shows only the Rosensweig instability ($\mathcal{N}_{c(\mathrm{Ro})} = 4.984$ and $k_{c(\mathrm{Ro})} = 0.779$) and no influence of heating can be noticed. When increasing $\mathcal{M}$ approximately to $0.97\mathcal{M}_{c(\mathrm{RBM})}$ one starts to notice a dip in the curve at a wave number, which belongs to that of thermal convection and which becomes deeper rapidly by increasing $\mathcal{M}$.

At a value of $\mathcal{M} = \mathcal{M}_{\mathrm{CD2}} = 0.9994\mathcal{M}_{c(\mathrm{RBM})}$ the system reaches a stationary codimension–2–point (CD2) with the critical parameters: $\mathcal{M}_{\mathrm{CD2}} = 78.438$, $k_{\mathrm{CD2(RBM)}} = 1.989$, $\mathcal{N}_{\mathrm{CD2}} = 4.961$ and $k_{\mathrm{CD2(Ro)}} = 0.779$. The inset in Figure 6, where the Rosensweig minimum is plotted with very high resolution (because of the high resolution only the four curves close to the CD2 are plotted), illustrates that for $0 < \mathcal{M} < \mathcal{M}_{\mathrm{CD2}}$ heating is suitable to decrease the threshold magnetisation of the Rosensweig instability slightly. In that case both destabilising mechanisms interfere and thus the Rosensweig mode is no longer purely static but now becomes dynamic. For $0.9994\mathcal{M}_{c(\mathrm{RBM})} < \mathcal{M} < \mathcal{M}_{c(\mathrm{RBM})}$ it is possible to reach the threshold of the Marangoni instability by means of applying a magnetic field. These possibilities to reduce the threshold values of the instabilities reflect the weak coupling between these both destabilising effects. In Figures 7 and 8 the corrections of the temperature– and velocity–field at the CD2 are plotted for the different wavenumbers $k_{\mathrm{CD2(Ro)}}$ and $k_{\mathrm{CD2(RBM)}}$ (colder regions are shown in a darker greyscale). The motion at the surface is – as it is expected from the Marangoni–effect – from warmer to colder regions. At the CD2 convection rolls are found for both wavenumbers,

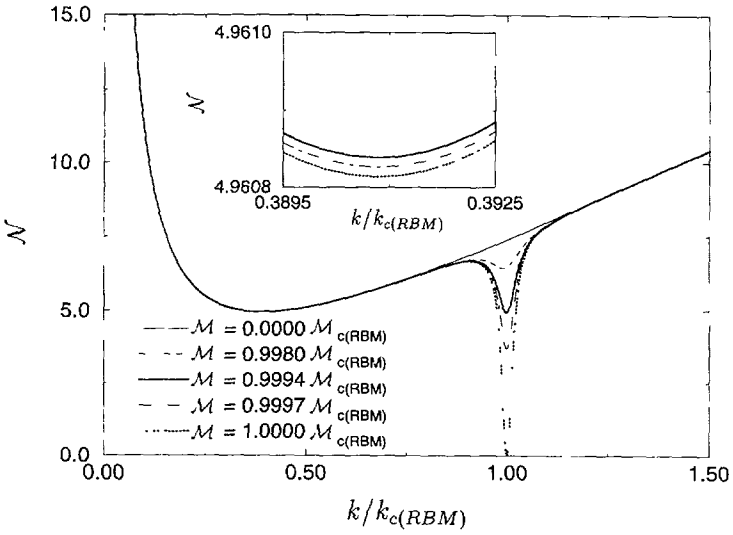

Fig. 6. — Neutral curves $\mathcal{N}(k)$ for various Marangoni numbers $\mathcal{M}$ ($\mathcal{M}_{c(RBM)} = 78.438$).

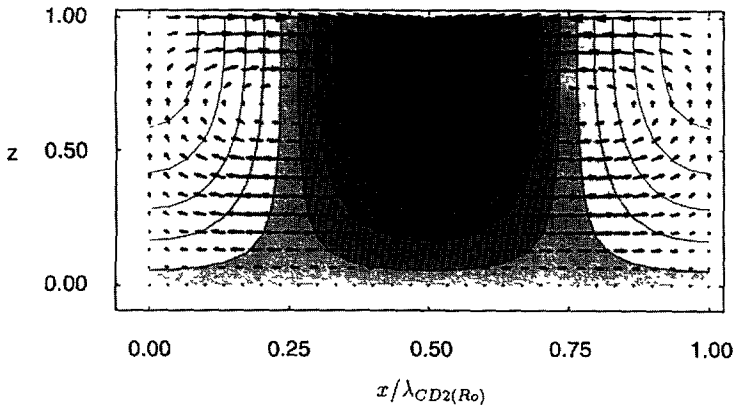

Fig. 7. — Corrections of the temperature field (darker grey scales denote colder regions) and corresponding velocity field at the CD2 ($k = k_{CD2(Ro)}$).

even though there is no motion at the onset of the pure Rosensweig instability, which stresses in an easily visible way the influence of thermoconvection on the Rosensweig instability at the linear stage through a modification of the corresponding eigenvector. In Figures 9 and 10 the corresponding corrections of the magnetic fields are plotted. These figures show the destabilising focusing of the magnetic field towards the wave crests induced by surface deflections.

When increasing $\mathcal{M}$ further, one reaches a regime, where the system becomes unstable against thermal convection, when an additional magnetic field is applied – but one has to mention, that this regime is quite small. At $\mathcal{M} = \mathcal{M}_{c(RBM)}$ the applied temperature gradient is large enough to drive thermal convection without an external field.

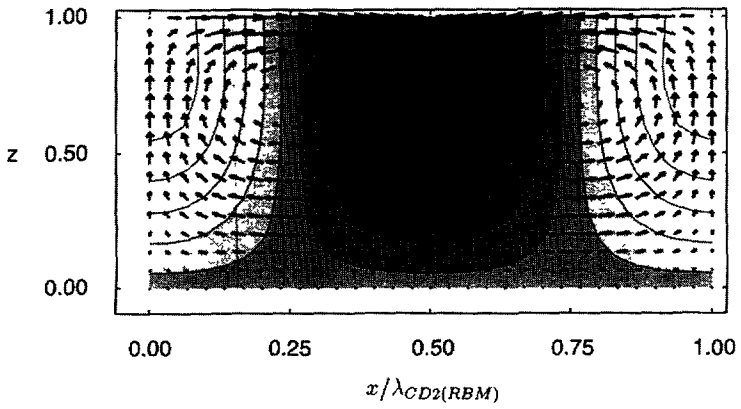

Fig. 8. — Corrections of the temperature field (darker grey scales denote colder regions) and corresponding velocity field at the CD2 ($k = k_{\mathrm{CD2(RBM)}}$).

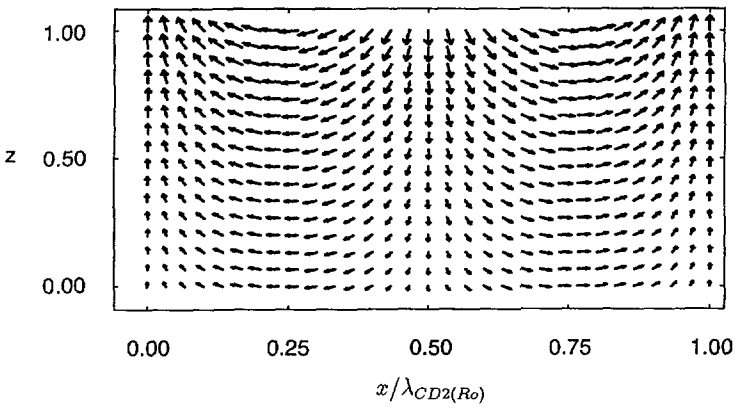

Fig. 9. — Corrections of the magnetic field at the CD2 ($k = k_{\mathrm{CD2(Ro)}}$).

To guarantee the existence of the CD2 for experimentally accessible conditions, we have to consider the influence of the Biot number $\mathcal{L}$, which is hard to evaluate. In Figure 11 neutral curves for the experimentally potentially interesting region $0.0003 \leq \mathcal{L} \leq 1.0$ are plotted. There is only a quantitative change of the critical parameters observed, but the CD2 still exists.
Since the wavelength of the Rosensweig peaks is determined predominantly by the properties of the magnetic fluid, whereas the wavelength of the convection rolls is essentially controlled by the thickness of the fluid layer, it is possible to move the latter by variations of d. In Figure 12 the neutral curves at the CD2 (when possible) are plotted for different values of d ($\mathcal{L} = 0.0003\ \mathrm{mm}^{-1}\ d$). For $d < 3$ mm the ratio between the $k_{\mathrm{CD2(Ro)}}$ and $k_{\mathrm{CD2(RBM)}}$ can be varied over a large range of values. At $d \approx 4$ mm the convection dip is inverted and gives rise to a local maximum as can be seen in Figure 12d. The question how the Bénard–Marangoni instability for thick layers ($d \gtrsim 4$ mm) arises as a limiting case is discussed in detail

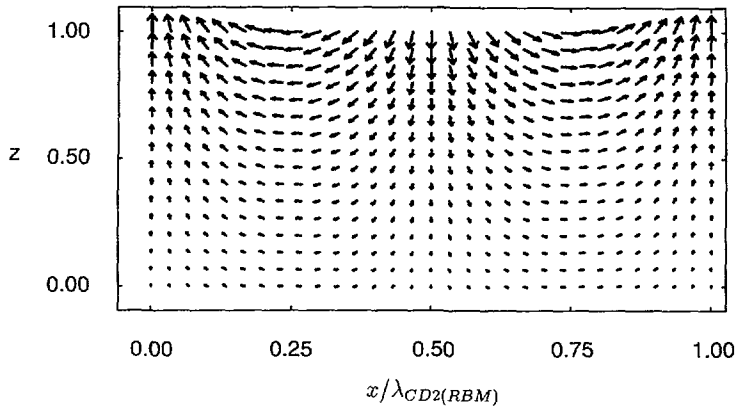

Fig. 10. — Corrections of the magnetic field at the CD2 ($k = k_{\mathrm{CD2(RBM)}}$).

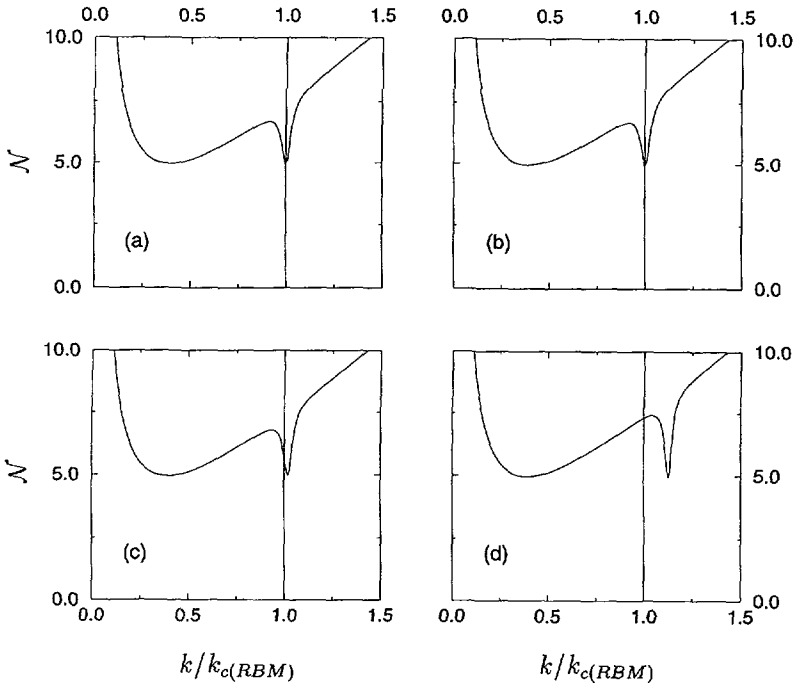

Fig. 11. — Neutral curves $\mathcal{N}(k)$ at the CD2 for increasing Biot numbers $\mathcal{L}$: (a) $\mathcal{L} = 0.0003$, $\mathcal{M} = 78.438$ and $\mathcal{R} = 10.056$; (b) $\mathcal{L} = 0.01$, $\mathcal{M} = 78.804$ and $\mathcal{R} = 10.103$; (c) $\mathcal{L} = 0.1$, $\mathcal{M} = 82.169$ and $\mathcal{R} = 10.534$ (d) $\mathcal{L} = 1.0$, $\mathcal{M} = 114.100$ and $\mathcal{R} = 14.627$.

in appendix B. In this appendix we also show the process of inversion. The inversion of the dip is not observed for $\mathcal{R} \equiv 0$. In this limiting case the location of the two minima can be varied over a large range. So the contributions of the Rayleigh–Bénard instability decide whether the system reaches a CD2 or not. Consequently this inversion of the peak is also observed, when increasing the Biot numbers to $\mathcal{L} > 50$ (which can probably not be reached in an experiment)

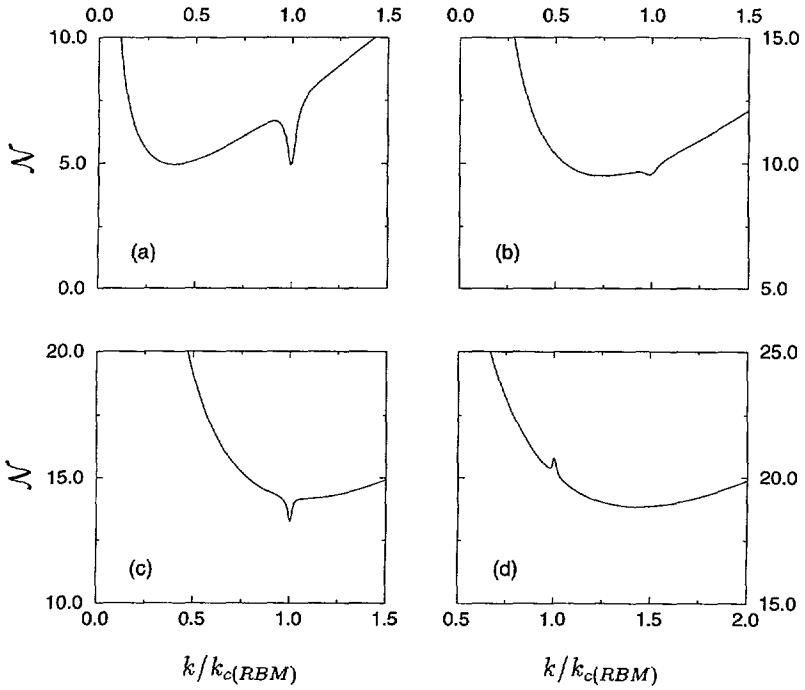

Fig. 12. — Neutral curves $\mathcal{N}(k)$ for increasing thickness of the layer d: (a) $d = 1\,\mathrm{mm}$, $\mathcal{M} = 78.486$ and $\mathcal{R} = 10.062$; (b) $d = 2\,\mathrm{mm}$, $\mathcal{M} = 75.353$ and $\mathcal{R} = 38.643$; (c) $d = 3\,\mathrm{mm}$, $\mathcal{M} = 70.596$ and $\mathcal{R} = 81.457$; (d) $d = 4\,\mathrm{mm}$, $\mathcal{M} = 64.800$ and $\mathcal{R} = 132.923$.

without change of d. As it is shown for example in [4] the critical Marangoni number increases by many orders of magnitude, when increasing the Biot number from the insulating ($\mathcal{L} = 0$) to the conducting case ($\mathcal{L} \to \infty$), whereas the critical Rayleigh number does not even double. Thus in the limit of high Biot numbers the contribution of buoyancy to thermal convection at the onset of instability is the dominant effect even for thin layers. So we can conclude, that the CD2 can only exist, when the influence of buoyancy is sufficiently small (e.g. small thickness or small Biot number).

4. Oscillatory Instability

Those effects discussed above, are only experimentally accessible, if there is no oscillatory instability which sets in at a lower threshold. To investigate this question, we solve the linearised equations (18) and (19) for $\omega \neq 0$ along with the corresponding boundary conditions (20)–(24). Following the usual procedure we obtain the neutral curve (cf. appendix C):

$$\mathcal{N}(k,\omega) = \frac{1}{\Lambda(k)k^3}\left[\left(\mathcal{B}+k^2\right)k^2 + h_{\mathcal{N}}(\mathcal{R},\mathcal{M},\mathcal{C},\mathcal{L},\mathcal{P},k,\omega)\right] , \tag{36}$$

or, when resolved for the Marangoni number:

$$\mathcal{M}(k,\omega) = -\frac{i\omega\mathcal{P}}{k^2}\cdot h_{\mathcal{M}}(\mathcal{R},\mathcal{N},\mathcal{C},\mathcal{L},\mathcal{P},k,\omega) \tag{37}$$

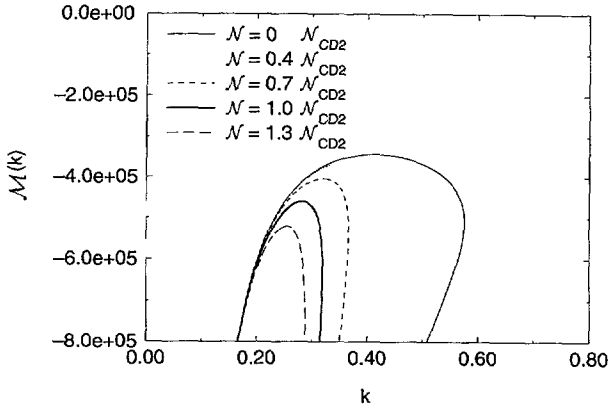

Fig. 13. — Neutral curves $\mathcal{M}(k)$ for the oscillatory instability for different magnetisation numbers $\mathcal{N}$ ($d = 1\,\mathrm{mm}$, $\mathcal{N}_{\mathrm{CD2}} = 4.961$ and $\mathcal{R} = 10.056$).

which are in general complex functions (the functions $h_{\mathcal{N}}$ and $h_{\mathcal{M}}$ are defined in the appendix C). Since the magnetisation number $\mathcal{N}$ (or the Marangoni number $\mathcal{M}$ respectively) is a measurable quantity, it has to be real. Thus a combination of the parameters k and ω has to be determined, so that the imaginary part of $\mathcal{N}(k,\omega)$ ($\mathcal{M}(k,\omega)$) vanishes. For further details cf. appendix C.

While calculating the neutral curve $\mathcal{M}(k,\omega)$ we have recovered the results of Takashima [8] for all the Prandtl numbers relevant for magnetic liquids.

We have investigated the intervals $10^{-10} \leq k \leq 100$ and $10^{-5} \leq \omega \leq 30$ in parameter space for $d = 1$ mm. In accordance with the experimental observations, we did not find an oscillatory branch for the pure Rosensweig instability.

In Figure 13 the neutral curves $\mathcal{M}(k,w)$ for different values of $\mathcal{N}$ are plotted. For increasing magnetisation numbers the threshold of an oscillatory instability also increases. Even without magnetic field we find a critical Marangoni number of $\mathcal{M} = -3.43 \times 10^5$, which corresponds to cooling the layer from below with a temperature gradient of -4×10^3 Kmm^{-1}, which is unreachable in an experiment.

Finally we return to the influence of the Biot number. Again we calculate the neutral curves $\mathcal{M}(k,w)$ for $\mathcal{L} = 0.0003$, $\mathcal{L} = 0.01$, $\mathcal{L} = 0.1$ and $\mathcal{L} = 1.0$ for $d = 1$ mm. In this range an increasing Biot number does not change the neutral curves qualitatively, but it has even a stabilising influence on the onset of the oscillatory instability (the corresponding critical Marangoni numbers for the parameters of the stationary CD2 are: $\mathcal{M}_{\mathrm{c}(\mathcal{L}=0.0003)} = -4.60 \times 10^5$, $\mathcal{M}_{\mathrm{c}(\mathcal{L}=0.01)} = -4.63 \times 10^5$, $\mathcal{M}_{\mathrm{c}(\mathcal{L}=0\,1)} = -4.97 \times 10^5$ and $\mathcal{M}_{\mathrm{c}(\mathcal{L}=1\,0)} = -1.96 \times 10^6$).

To sum up, we can state that under experimentally relevant conditions there is no oscillatory instability, which would set in with a lower threshold and would thus destroy the existence of the stationary CD2 point discussed above.

5. Conclusions

We have systematically studied the linear stability properties of a magnetic fluid with deformable free surface heated from below and exposed to a vertical magnetic field. For thin layers (Marangoni-dominated regime) we have found a stationary codimension-2-point with quite different critical wavenumbers. We have calculated the eigenfunctions at the CD2 and found convection rolls at both wavenumbers, whereas the pure Rosensweig instability sets in

with vanishing velocity. Using the physical data of a magnetic fluid, that is commercially available, we have shown that the critical parameters of the CD2 can be reached in an experiment (for a layer which has a thickness of 1 mm, the necessary temperature gradient is about 1 Kmm^{-1} and the critical magnetic induction about 10^{-2} T). We have discussed the influence of the thermal boundary conditions, which can have a drastic influence on the relative contributions of the driving mechanisms for thermal convection. From a stability analysis for the oscillatory case, we have shown that there is no oscillatory instability, that would set in at a lower threshold and would thus make the CD2 unreachable.

While the Rosensweig instability is an intrinsic instability of the fluid, whose critical wavelength is nearly independent of layer thickness, the critical wavelength of the thermal instabilities is strongly dependent on the thickness of the fluid layer. Taking this fact into account, we have proposed a variation of the ratio of the two critical wavenumbers by varying the thickness of the layer, which can induce a significant change in the patterns the system generates. While doing this one has to keep in mind that when buoyancy effects become dominant, i.e. when d is bigger than about $3-4$ mm, the CD2 does not exist anymore.

Since we have focused in this manuscript on a linear theory, we cannot evaluate the amplitude of the eigenfunctions or make predictions about the pattern, that will actually be observed in the vicinity of the CD2 above onset. The system could choose between any spatial superposition of the two linearly unstable modes with quite different wavelengths. One possibility is, that the system forms more complex patterns with two length scales, like e.g. rectangles. Another possibility would be a mixed state as it has been considered for convective onset in viscoelastic liquids by Brand and Zielinska [24]. Since the ratio of the critical wavenumbers is in general not an integer number, the resulting structure could then become rather complex giving rise to incommensurate patterns. Since, as has been discussed above, the ratio between the two critical wavenumbers can be varied in a certain range by changing the layer thickness d one can achieve, that the wavenumber ratio becomes an integer number thus opening the possibility to study spatial resonance and lock-in phenomena near the onset of an instability.

Acknowledgments

H.R.B. thanks the Deutsche Forschungsgemeinschaft for partial support of his work through the Graduiertenkolleg "Nichtlineare Spektroskopie und Dynamik". It is a pleasure for J.W. to thank Thomas Mahr for stimulating discussions and for sharing with me his experimental results.

Appendix A

Stationary Instability

The bulk equations (18) and (19) for stationary instability ($\omega = 0$) reduce to the following linear differential equation of sixth order (well known from Rayleigh–Bénard instability [18]):

$$\left(D^2 - k^2\right)^3 \hat{\theta}_1 = -\mathcal{R} k^2 \hat{\theta}_1 \,. \tag{A.1}$$

The solution for $\mathcal{R} \neq 0$ of equation (A.1) can be written in the following form:

$$\hat{\theta}_1 = \sum_{i=1}^{3} A_i \sinh\left(\lambda_i z\right) + B_i \cosh\left(\lambda_i z\right) \tag{A.2}$$

with the roots of the characteristic polynomial of equation (A.1):

$$\lambda_1 = -\sqrt[3]{Rk^2} + k^2 \qquad \lambda_{2,3} = \frac{1}{2}\left(1 \pm i\sqrt{3}\right)\sqrt[3]{Rk^2} + k^2 \tag{A.3}$$

All but one of the coefficients A_i and B_i can determined by the boundary conditions (20) and (24). The solvability condition of the resulting set of homogeneous linear equations reads:

$$\begin{vmatrix} 1 & 1 & 1 & 0 & 0 & 0 \\ E_1 & E_2 & E_3 & 0 & 0 & 0 \\ 0 & 0 & 0 & F_1 & F_2 & F_3 \\ E_4 & E_5 & E_6 & E_7 & E_8 & E_9 \\ E_{10} & E_{11} & E_{12} & E_{13} & E_{14} & E_{15} \\ F_4 & F_5 & F_6 & F_7 & F_8 & F_9 \end{vmatrix} = 0 \tag{A.4}$$

with the following abbreviations ($i = 1, 2, 3$):

$$\begin{aligned} E_i &= k^2 - \lambda_i^2 \qquad E_{i+3} = E_i \cosh(\lambda_i) \qquad E_{i+6} = E_i \sinh(\lambda_i) \\ E_{i+9} &= \lambda_i \sinh(\lambda_i) - \frac{\mathcal{L}}{\mathcal{M}k^2}\lambda_i^2 E_i \cosh(\lambda_i) \qquad E_{i+12} = \lambda_i \cosh(\lambda_i) - \frac{\mathcal{L}}{\mathcal{M}k^2}\lambda_i^2 E_i \sinh(\lambda_i) \\ F_i &= \lambda_i E_i \qquad F_{i+3} = \lambda_i \left\{ \mathcal{C}\left(3k^2 - \lambda_i^2\right) E_i + \frac{\Gamma}{\mathcal{L}} \right\} \sinh(\lambda_i) + \Gamma \cosh(\lambda_i) \\ F_{i+6} &= \lambda_i \left\{ \mathcal{C}\left(3k^2 - \lambda_i^2\right) E_i + \frac{\Gamma}{\mathcal{L}} \right\} \cosh(\lambda_i) + \Gamma \sinh(\lambda_i) \\ \Gamma &= \left(\mathcal{B} + k^2\right) k^2 - \mathcal{N}\Lambda(k) k^3 \end{aligned}$$

Expanding the determinant in equation (A.4) yields the neutral curve for marginal stability:

$$\mathcal{N}(k) = \frac{1}{\Lambda(k)k^3}\left[\left(\mathcal{B} + k^2\right) k^2 + \underbrace{\frac{\mathcal{C}\sum_{i=1}^{4} G_i D_i}{\sum_{i=1}^{4} H_i D_i}}_{= g(\mathcal{R}, \mathcal{M}, \mathcal{C}, \mathcal{L}, k)} \right] \tag{A.5}$$

with:

$$\begin{aligned} G_1 &= \lambda_1\left(3k^2 - \lambda_1^2\right) E_1 \sinh(\lambda_1) - \lambda_2\left(3k^2 - \lambda_2^2\right) E_2 \sinh(\lambda_2) \\ G_2 &= \lambda_3\left(3k^2 - \lambda_3^2\right) E_3 \sinh(\lambda_3) - \lambda_1\left(3k^2 - \lambda_1^2\right) E_1 \sinh(\lambda_1) \\ G_3 &= \frac{F_1}{F_3}\lambda_3\left(3k^2 - \lambda_3^2\right) E_3 \cosh(\lambda_3) - \lambda_1\left(3k^2 - \lambda_1^2\right) E_1 \cosh(\lambda_1) \\ G_4 &= \lambda_2\left(3k^2 - \lambda_2^2\right) E_2 \cosh(\lambda_2) - \frac{F_2}{F_3}\lambda_3\left(3k^2 - \lambda_3^2\right) E_3 \cosh(\lambda_3) \\ H_1 &= \frac{\lambda_1}{\mathcal{L}}\sinh(\lambda_1) - \frac{\lambda_2}{\mathcal{L}}\sinh(\lambda_2) + \cosh(\lambda_1) - \cosh(\lambda_2) \end{aligned}$$

$$
\begin{aligned}
H_2 &= \frac{\lambda_3}{\mathcal{L}}\sinh(\lambda_3) - \frac{\lambda_1}{\mathcal{L}}\sinh(\lambda_1) + \cosh(\lambda_3) - \cosh(\lambda_1) \\
H_3 &= \frac{F_1}{F_3}\left[\frac{\lambda_3}{\mathcal{L}}\cosh(\lambda_3) + \sinh(\lambda_3)\right] - \frac{\lambda_1}{\mathcal{L}}\cosh(\lambda_1) - \sinh(\lambda_1) \\
H_4 &= \frac{\lambda_2}{\mathcal{L}}\cosh(\lambda_2) + \sinh(\lambda_2) - \frac{F_2}{F_3}\left[\frac{\lambda_3}{\mathcal{L}}\cosh(\lambda_3) + \sinh(\lambda_3)\right]
\end{aligned}
$$

and the minors:

$$
\begin{aligned}
D_1 &= (E_3 - E_1)\left[\left(E_7 - \frac{E_9F_1}{F_3}\right)\left(E_{14} - \frac{F_2F_3}{E_{15}}\right) - \left(E_8 - \frac{E_9F_2}{F_3}\right)\left(E_{13} - \frac{F_1E_{15}}{F_3}\right)\right] \\
D_2 &= (E_2 - E_1)\left[\left(E_7 - \frac{E_9F_1}{F_3}\right)\left(E_{14} - \frac{F_2F_3}{E_{15}}\right) - \left(E_8 - \frac{E_9F_2}{F_3}\right)\left(E_{13} - \frac{F_1E_{15}}{F_3}\right)\right] \\
D_3 &= (E_2 - E_1)\left[(E_6 - E_4)\left(E_{14} - \frac{F_2E_{15}}{F_3}\right) - \left(E_8 - \frac{E_9F_2}{F_3}\right)(E_{12} - E_{10})\right] \\
&\quad - (E_3 - E_1)\left[(E_5 - E_4)\left(E_{14} - \frac{F_2E_{15}}{F_3}\right) - \left(E_8 - \frac{E_9F_2}{F_3}\right)(E_{11} - E_{10})\right] \\
D_4 &= (E_2 - E_1)\left[(E_6 - E_4)\left(E_{13} - \frac{F_1E_{15}}{F_3}\right) - \left(E_7 - \frac{E_9F_1}{F_3}\right)(E_{12} - E_{10})\right] \\
&\quad - (E_3 - E_1)\left[(E_5 - E_4)\left(E_{13} - \frac{F_1E_{15}}{F_3}\right) - \left(E_7 - \frac{E_9F_1}{F_3}\right)(E_{11} - E_{10})\right] \qquad \text{(A.6)}
\end{aligned}
$$

Appendix B

Transition from 'Thin' to 'Thick' Layers

Here we argue how the Bénard–Marangoni instability emerges as a limiting case in the regime of thick layers ($d \gtrsim 4$ mm). We also discuss the conversion process of the Marangoni minimum in the neutral curve $\mathcal{N}(k)$ into a maximum.

As can be seen from Figure 12d at $d \approx 4$ mm the Marangoni minimum is inverted towards a sharp maximum. This peak reacts very sensitively on an increase of $\mathcal{M}$ and then it diverges ($\mathcal{N}(k = k_{(\mathrm{RBM})}) \to \infty$). As a consequence a maximum appears from $\mathcal{N} = -\infty$, which touches the k–axis at a certain value of $\mathcal{M}$ (cf. Fig. 14). Since negative values of $\mathcal{N}$ cannot be reached in a physical system by construction of $\mathcal{N}$, the first physically accessible value for $\mathcal{N}$ has to be zero. This zero of $\mathcal{N}(k)$ determines the threshold for thermoconvection. For $d = 4$ mm all of that happens in a small interval between $\mathcal{M} = 64.800$ and $\mathcal{M} = 64.809$.

At the thickness of $d = 3.628$ mm the dip changes its direction. The system achieves this, by creating a local minimum and in the close neighborhood a local maximum, which at first sight seems to be a singularity, as can be seen in Figure 15. Since both the minimum and the maximum react very sensitively on an increase of $\mathcal{M}$, this is a way for the system to change from a regime of thicknesses that allow a CD2 to exist, towards one for which there is no CD2, without reaching a point, where no thermal convection sets in. The latter needs to be accessible to guarantee, that the system shows thermoconvection for each layer thickness, when no magnetic field but a sufficiently high temperature gradient is applied.

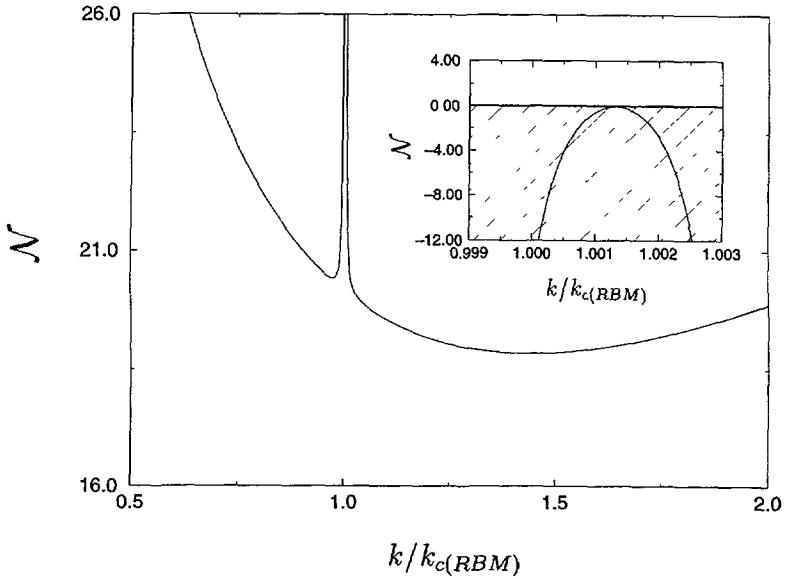

Fig. 14. — Neutral curve $\mathcal{N}(k)$ that describes the onset of thermal convection in a 'thick' layer ($d = 4\,\text{mm}$, $\mathcal{M} = 64.809$ and $\mathcal{R} = 132.942$). The hatched region is a physically inaccessible region in parameter space.

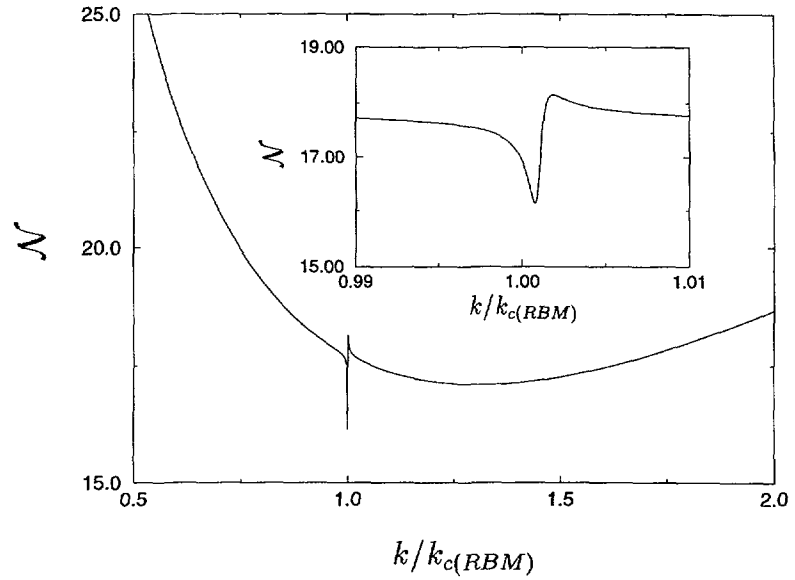

Fig. 15. — Neutral curve $\mathcal{N}(k)$ at the transition from thin to thick layers ($d = 3.628\,\text{mm}$, $\mathcal{M} = 67.043$ and $\mathcal{R} = 113.135$).

Appendix C

Oscillatory Instability

In the case of $\omega \neq 0$ equations (18) and (19) can be combined to the equation:

$$\left(D^2 - k^2\right)\left(D^2 - k^2 - i\omega\right)\left(i\omega\mathcal{P} - D^2 + k^2\right)\hat{\theta}_1(z) \;=\; \mathcal{R}k^2\hat{\theta}_1(z)\,, \tag{C.1}$$

which we solve for $\mathcal{R} \neq 0$ and $\mathcal{P} \neq 1$ with the ansatz:

$$\hat{\theta}_1(z) \;=\; \sum_{i=1}^{3}\left[A_i \cosh(\lambda_i z) \;+\; B_i \sinh(\lambda_i z)\right]\,. \tag{C.2}$$

Since the roots λ_i of the characteristic polynomial of equation (C.1) for $\mathcal{R} \neq 0$ cannot be calculated analytically, we determine them by means of the fortran routine LAGUER from *Numerical Recipes* [25]. With the boundary conditions (20)–(24), we get a set of linear equations. The solvability condition yields again a determinant of the structure of equation (A.4) with the modified abbreviations:

$$\begin{aligned}
E_i &= i\omega\mathcal{P} - \lambda_i^2 + k^2 \\
E_{i+3} &= \lambda_i \sinh(\lambda_i) + \frac{\mathcal{L}}{i\omega\mathcal{P}}\left(\lambda_i^2 - k^2\right)\cosh(\lambda_i) \\
E_{i+6} &= \lambda_i \cosh(\lambda_i) + \frac{\mathcal{L}}{i\omega\mathcal{P}}\left(\lambda_i^2 - k^2\right)\sinh(\lambda_i) \\
E_{i+9} &= \left\{i\omega\mathcal{P}\left(\lambda_i^2 + k^2\right) + \left[\left(\frac{\mathcal{M}}{i\omega\mathcal{P}} - 1\right)k^2 - \lambda_i^2\right]\left(\lambda_i^2 - k^2\right)\right\}\cosh(\lambda_i) \\
E_{i+12} &= \left\{i\omega\mathcal{P}\left(\lambda_i^2 + k^2\right) + \left[\left(\frac{\mathcal{M}}{i\omega\mathcal{P}} - 1\right)k^2 - \lambda_i^2\right]\left(\lambda_i^2 - k^2\right)\right\}\sinh(\lambda_i) \\
F_i &= \lambda_i E_i \\
F_{i+3} &= E_i\left\{\mathcal{C}\left(i\omega - \lambda_i^2 + 3k^2\right)\lambda_i \sinh(\lambda_i) \;+\; \frac{\Gamma}{i\omega\mathcal{P}}\cosh(\lambda_i)\right\} \\
F_{i+6} &= E_i\left\{\mathcal{C}\left(i\omega - \lambda_i^2 + 3k^2\right)\lambda_i \cosh(\lambda_i) \;+\; \frac{\Gamma}{i\omega\mathcal{P}}\sinh(\lambda_i)\right\}\,,
\end{aligned} \tag{C.3}$$

where Γ is defined as in appendix A.
The neutral curve reads:

$$\mathcal{N}(k,\omega) = \frac{1}{\Lambda(k)k^3}\left[\left(\mathcal{B} + k^2\right)k^2 + \underbrace{i\omega\mathcal{C}\mathcal{P}\,\frac{\sum_{i=1}^{4} G_i D_i}{\sum_{i=1}^{4} H_i D_i}}_{= h_{\mathcal{N}}(\mathcal{R},\mathcal{M},\mathcal{C},\mathcal{L},\mathcal{P},k,\omega)}\right] \tag{C.4}$$

with:
$$\begin{aligned}
G_1 &= \lambda_1\left(i\omega + 3k^2 - \lambda_1^2\right)E_1 \sinh(\lambda_1) - \lambda_2\left(i\omega + 3k^2 - \lambda_2^2\right)E_2 \sinh(\lambda_2) \\
G_2 &= \lambda_3\left(i\omega + 3k^2 - \lambda_3^2\right)E_3 \sinh(\lambda_3) - \lambda_1\left(i\omega + 3k^2 - \lambda_1^2\right)E_1 \sinh(\lambda_1)
\end{aligned}$$

$$
\begin{aligned}
G_3 &= \frac{F_1}{F_3}\lambda_3\left(i\omega+3k^2-\lambda_3^2\right)E_3\cosh(\lambda_3)-\lambda_1\left(i\omega+3k^2-\lambda_1^2\right)E_1\cosh(\lambda_1)\\
G_4 &= \lambda_2\left(i\omega+3k^2-\lambda_2^2\right)E_2\cosh(\lambda_2)-\frac{F_2}{F_3}\lambda_3\left(i\omega+3k^2-\lambda_3^2\right)E_3\cosh(\lambda_3)\\
H_1 &= E_1\cosh(\lambda_1)-E_2\cosh(\lambda_2) \qquad H_2 = E_3\cosh(\lambda_3)-E_1\cosh(\lambda_1)\\
H_3 &= \frac{F_1E_3}{F_3}\sinh(\lambda_3)-E_1\sinh(\lambda_1) \qquad H_4 = E_2\sinh(\lambda_2)-\frac{F_2E_3}{F_3}\sinh(\lambda_3)\,.
\end{aligned}
$$

The minors are defined in the same way as in equation (A.6), but incorporating the redefined E_i's and F_i's.
For the oscillatory instability it is also suitable to calculate the neutral curve $\mathcal{M}(k,\omega)$:

$$
\mathcal{M}(k,\omega) = -\frac{i\omega\mathcal{P}}{k^2}\cdot\underbrace{\frac{\sum_{i=1}^{3}E_iK_i\left(\lambda_i^2+k^2\right)}{\sum_{i=1}^{3}K_i\left(\lambda_i^2-k^2\right)}}_{=h_{\mathcal{M}}(\mathcal{R},\mathcal{N},\mathcal{C},\mathcal{L},\mathcal{P},k,\omega)} \tag{C.5}
$$

with:

$$
K_1 = \cosh(\lambda_1)\hat{D}_1-\cosh(\lambda_1)\hat{D}_2-\sinh(\lambda_1)\hat{D}_3 \tag{C.6}
$$

$$
K_2 = \sinh(\lambda_2)\hat{D}_4-\cosh(\lambda_2)\hat{D}_1 \tag{C.7}
$$

$$
K_3 = \cosh(\lambda_3)\hat{D}_2+\sinh(\lambda_3)\frac{F_1\hat{D}_3}{F_3}-\sinh(\lambda_3)\frac{F_2\hat{D}_4}{F_3} \tag{C.8}
$$

and the minors:

$$
\begin{aligned}
\hat{D}_1 &= (E_3-E_1)\left[\left(E_7-\frac{E_9F_1}{F_3}\right)\left(F_8-\frac{F_2F_9}{F_3}\right)-\left(E_8-\frac{E_9F_2}{F_3}\right)\left(F_7-\frac{F_1F_9}{F_3}\right)\right]\\
\hat{D}_2 &= (E_2-E_1)\left[\left(E_7-\frac{E_9F_1}{F_3}\right)\left(F_8-\frac{F_2F_9}{F_3}\right)-\left(E_8-\frac{E_9F_2}{F_3}\right)\left(F_7-\frac{F_1F_9}{F_3}\right)\right]\\
\hat{D}_3 &= (E_2-E_1)\left[(E_6-E_4)\left(F_8-\frac{F_2F_9}{F_3}\right)-\left(E_8-\frac{E_9F_2}{F_3}\right)(F_6-F_4)\right]-\\
&\quad-(E_3-E_1)\left[(E_5-E_4)\left(F_8-\frac{F_2F_9}{F_3}\right)-\left(E_8-\frac{E_9F_2}{F_3}\right)(F_5-F_4)\right]\\
\hat{D}_4 &= (E_2-E_1)\left[(E_6-E_4)\left(F_7-\frac{F_1F_9}{F_3}\right)-\left(E_7-\frac{E_9F_1}{F_3}\right)(F_6-F_4)\right]-\\
&\quad-(E_3-E_1)\left[(E_5-E_4)\left(F_7-\frac{F_1F_9}{F_3}\right)-\left(E_7-\frac{E_9F_1}{F_3}\right)(F_5-F_4)\right]
\end{aligned} \tag{C.9}
$$

References

[1] Lord Rayleigh, *Philos. Mag.* **32** (1916) 529.
[2] Bénard H., *Rev. Gen. Sci. Pur. Appl.* **11** (1900) 1261.
[3] Pearson J.R.A., *J. Fluid Mech.* **4** (1958) 489.
[4] Nield D.A., *J. Fluid Mech.* **19** (1964) 341.
[5] Scriven L.E., Sternling C.V., *J. Fluid Mech.* **19** (1961) 321.
[6] Smith K.A., *J. Fluid Mech.* **24** (1966) 401.
[7] Takashima M., *J. Phys. Soc. Jpn.* **50** (1981) 2745.
[8] Takashima M., *J. Phys. Soc. Jpn.* **50** (1981) 2751.
[9] Pérez-Garcia C., Carneiro G., *Phys. Fluids* **A3** (1991) 292.
[10] Benguria R.D., Depassier M.C., *Phys. Fluids* **A30** (1987) 1678.
[11] Benguria R.D., Depassier M.C., *Phys. Fluids* **A1** (1989) 1123.
[12] Rosensweig R.E., Ferrohydrodynamics (Cambridge, London, 1985).
[13] Rosensweig R.E., *Ann. Rev. Fluid Mech.* **19** (1987) 437.
[14] Cowley M.D., Rosensweig R.E., *J. Fluid Mech.* **30** (1967) 671.
[15] Néron de Surgy G., Chabrerie J.-P., Denoux O., Wesfreid J.E., *J. Phys. II France* **3** (1993) 1201.
[16] Schwab L., PhD Thesis, University of Munich, unpublished (1989).
[17] Schwab L., *J. Magn. Magn. Mat.* **85** (1990) 199.
[18] Chandrasekhar S., Hydrodynamic and Hydromagnetic Stability (Oxford University Press, Oxford 1961).
[19] Lebon G., Cloot A., *Act. Mech.* **43** (1982) 141.
[20] Salin D., *Europhys. Lett.* **21** (1993) 667.
[21] Data provided by AT&P Ferrofluidics, Nürtingen.
[22] Mahr T., Groisman A., Rehberg I., preprint 9/95
[23] The Biot number (and most of the other dimensionless numbers of this system) depends on the physical data of the fluid and on the thickness of the fluid layer d. In order to investigate the influence of d on the neutral curve, the Biot number and all the dimensionless parameters in table I are listed as functions of d. Only the Prandtl number is independent of d.
[24] Brand H.R., Zielinska B.J.A., *Phys. Rev. Lett.* **57** (1986) 3167.
[25] Press W.H., Flannery B.P., Teukolsky S.A., Vetterling W.T., Numerical Recipes (Cambridge University Press, London 1986).